


# Two Possible Side Reaction Pathways during Furanic Etherification

Wenting Fang , Hualei Hu, Zhongsen Ma, Lei Wang and Yajie Zhang \*

Key Laboratory of Bio-based Polymeric Materials Technology and Application of Zhejiang Province, Ningbo Institute of Materials Technology & Engineering, Chinese Academy of Sciences, 1219 Zhongguan West Road, Ningbo 315021, China; fangwentong@nimte.ac.cn (W.F.); huhualei@nimte.ac.cn (H.H.); mazu@nimte.ac.cn (Z.M.); wanglei@nimte.ac.cn (L.W.)

\* Correspondence: zhangyj@nimte.ac.cn; Tel.: +86-0574-8669-0283

Received: 16 August 2018; Accepted: 6 September 2018; Published: 8 September 2018



**Abstract:** The revealing mechanism of side reactions is crucial for obtaining theoretical yield in industrialization when 2,5-bis(methoxymethyl)furan (BMMF) yield is above 95%. By-products catalyzed by the conventional ZSM-5 (C-ZSM-5) and hierarchical porous ZSM-5 (HP-ZSM-5) catalytic systems were different, and some key by-products were identified. Thus, possible pathways were proposed, which helps to further improve BMMF selectivity. Additionally, HP-ZSM-5 exhibited quicker reaction rate, higher BMMF yield and selectivity, and slower deactivation process. The relatively weak acidity of HP-ZSM-5 suppresses the ring-opening reaction and subsequent side reactions, and introduction of mesopores improves mass transport and slightly increases hydration of 2,5-bis(hydroxymethyl)furan (BHMF).

**Keywords:** etherification; furanic diether; heterogeneous catalysis; side reaction; ZSM-5

## 1. Introduction

Furanic diethers, potential alternatives of biofuels or diesel additives, can protect the environment by reducing CO<sub>2</sub>, NO<sub>x</sub>, and SO<sub>x</sub> emission [1–3]. For example, up to 40 vol % of 5-(*tert*-butoxymethyl)furfural (*t*-BMF) can mix with commercial diesel without any flocculation problems and also increases the cetane number [4]. The European Stationary Cycle test has already revealed that 2,5-bis(ethoxymethyl)furan (BEMF) has no significant difference in engine operation for all tested blending ratios [1]. Thus, obtaining highly efficient production of 2,5-bis(alkoxymethyl)furan (BAMF) is vital for the future industrialization.

Some works have been conducted about furanic diethers synthesis, especially about 2,5-bis(methoxymethyl)furan (BMMF), a typical furanic diether. Lee et al. studied the catalytic activity of Amberlyst-15 in the etherification of 2,5-bis(hydroxymethyl)furan (BHMF) with methanol, and attained 57% BMMF yield [5]. Cao et al. reported that both BMMF yield and selectivity were 70% by using ZSM-5 as catalyst [6]. Gupta et al. used a sulfonated carbocatalyst to catalyze BHMF to form BMMF and gained an 89% yield of BMMF [7]. Although solid acid catalysts are different, the above results demonstrate that side reactions are the main reason for low selectivity and yield. Recently, 98.5% BMMF yield was obtained by using reduced Co<sub>3</sub>O<sub>4</sub> as catalyst, which is higher than that of other solid acid catalysts [8]. However, there is still 1.5% by-products.

It is well known that solid acid catalysts have been widely employed in industrial etherification process. In order to match current equipment in etherification industry, solid acid, particularly porous catalyst, will be the best choice in the industrial process of furanic etherification [9]. Among the porous catalysts, ZSM-5 is an appropriate choice, because kinetic diameters of BHMF and BMMF are very close to the pore diameter of ZSM-5 [10,11], and shape selectivity of ZSM-5 might improve BMMF

selectivity. Meanwhile, introduction of mesopores to ZSM-5 can also increase selectivity of main product, relieve coke deposition, and enhance catalyst stability [12,13].

As is known to all, coke deposition derived from side reactions severely affects porous catalyst life time [14]. Meanwhile, given high yield is obtained, selectivity is key factor in industry. There are some possible side reaction pathways during BHMF etherification. Gelmini et al. proposed that BHMF itself occurred hydration reaction [15]. And furan ring is prone to open and polymerize under acidic condition [16–18]. Additionally, side reactions affect subsequent purification and waste treatment, which determines product cost. Thus, it is important to analyze and explore mechanism of side reactions over ZSM-5 to improve selectivity of main product.

In this work, our aim is to further explore the mechanism of side reactions over ZSM-5 during BHMF etherification by comparing catalytic performance of C-ZSM-5 and HP-ZSM-5. And HP-ZSM-5 showed quicker reaction rate, higher BMMF yield and selectivity, and slower deactivation than that of C-ZSM-5, which may lead to different by-products and side reaction mechanisms. Thus, we compared by-products in the C-ZSM-5 and HP-ZSM-5 catalytic systems, and identified some of key by-products. Two possible side reaction pathways were proposed in terms of the previous reports and our results.

## 2. Results and Discussion

### 2.1. Catalyst Characterization

X-ray diffraction (XRD) results show that all patterns of two catalysts are consistent with the reported Mobil Five (MFI)-structured materials [19], and no additional crystalline phases are observed (Figure S1). C-ZSM-5 displays type-I isotherms (plateau at relative pressure and without hysteresis) (Figure S2), which is common for microporous materials with relatively low external surface areas [20]. In contrast, the curve of HP-ZSM-5 is categorized as a type-IV isotherm, associated with capillary condensation occurring in the mesopores [21]. Moreover, HP-ZSM-5 possesses a mesopore size distribution between 3 nm and 5 nm (Figure S2), and an obvious increase in the mesopore volume compared to C-ZSM-5 (Table 1).

Table 1 and Figure S3 show that the acidity of HP-ZSM-5 is significantly weaker than that of C-ZSM-5. Some researchers also reported that the acid strength of sites located on mesopore external surface is lower than strength of the acid sites limited inside the zeolite micropores, therefore, hierarchical porous ZSM-5 often displays relatively weaker acidity than microporous ZSM-5 [22,23]. The above characteristics show that C-ZSM-5 and HP-ZSM-5 have similar micropore volume but HP-ZSM-5 has higher mesopore volume and lower acidity.

**Table 1.** The physico-chemical properties of the samples.

Sample	Si/Al Molar Ratio <sup>a</sup>	$S_{\text{BET}}$ ( $\text{m}^2 \cdot \text{g}^{-1}$ ) <sup>b</sup>	$V_{\text{micro}}$ ( $\text{cm}^3 \cdot \text{g}^{-1}$ ) <sup>c</sup>	$V_{\text{meso}}$ ( $\text{cm}^3 \cdot \text{g}^{-1}$ ) <sup>d</sup>	Number of Acid Sites ( $\text{mmol of NH}_3 \cdot \text{g}^{-1}$ ) <sup>e</sup>		
					Weak Acid	Strong Acid	Total Acid
Conventional ZSM-5 (C-ZSM-5)	33	330	0.11	0.05	0.33	0.43	0.76
Hierarchical porous ZSM-5 (HP-ZSM-5)	43	453	0.11	0.34	0.14	0.16	0.30

<sup>a</sup> Determined by X-ray fluorescence (XRF). <sup>b</sup> Calculated by Brunauer–Emmett–Teller (BET) method. <sup>c</sup> Estimated by the t-plot method. <sup>d</sup> Calculated by a subtraction of the total pore volume at a relative pressure of  $P/P_0 = 0.99$  from the t-plot method. <sup>e</sup> Determined by  $\text{NH}_3$  desorption (chemisorbed at 100 °C). Two peaks are shown in Figure S3, which are attributed to the ammonia absorbed on the weak and strong acid sites, respectively.

## 2.2. Catalytic Performance of C-ZSM-5 and HP-ZSM-5 in the Etherification of BHMF

C-ZSM-5 and HP-ZSM-5 were employed to catalyze etherification of BHMF with methanol. Obviously, conversion of BHMF over HP-ZSM-5 is much faster than that of C-ZSM-5 in Figure 1. For C-ZSM-5, BHMF is always detected during the reaction process even if the reaction time extends to 24 h. 5-Methoxymethyl furfural alcohol (MMFA) yield quickly increases, and then gradually decreases. The MMFA consumption rate of C-ZSM-5 is much slower than that of HP-ZSM-5. There is still 18% MMFA in C-ZSM-5 catalytic system when the reaction completes, which is one of reasons of low BMMF yield. BMMF yield of HP-ZSM-5 (94.5%) is much higher than that of C-ZSM-5 (63.7%). As shown in Table 1 and Figure S3, acidity of C-ZSM-5 is nearly 2.5 times higher than that of HP-ZSM-5. However, HP-ZSM-5 shows much higher activity, including faster reaction rate and higher BMMF yield, suggesting that HP-ZSM-5 may have more accessible active acid sites. Some evidences manifest that the role of micropores is controlling shape-selectivity and the function of mesopores is enhancing transport of reactants and products [24]. Introduction of mesopores can increase the number of accessible micropores and reduce the diffusion path [25]. Therefore, HP-ZSM-5 is more active than C-ZSM-5 in the BHMF etherification.

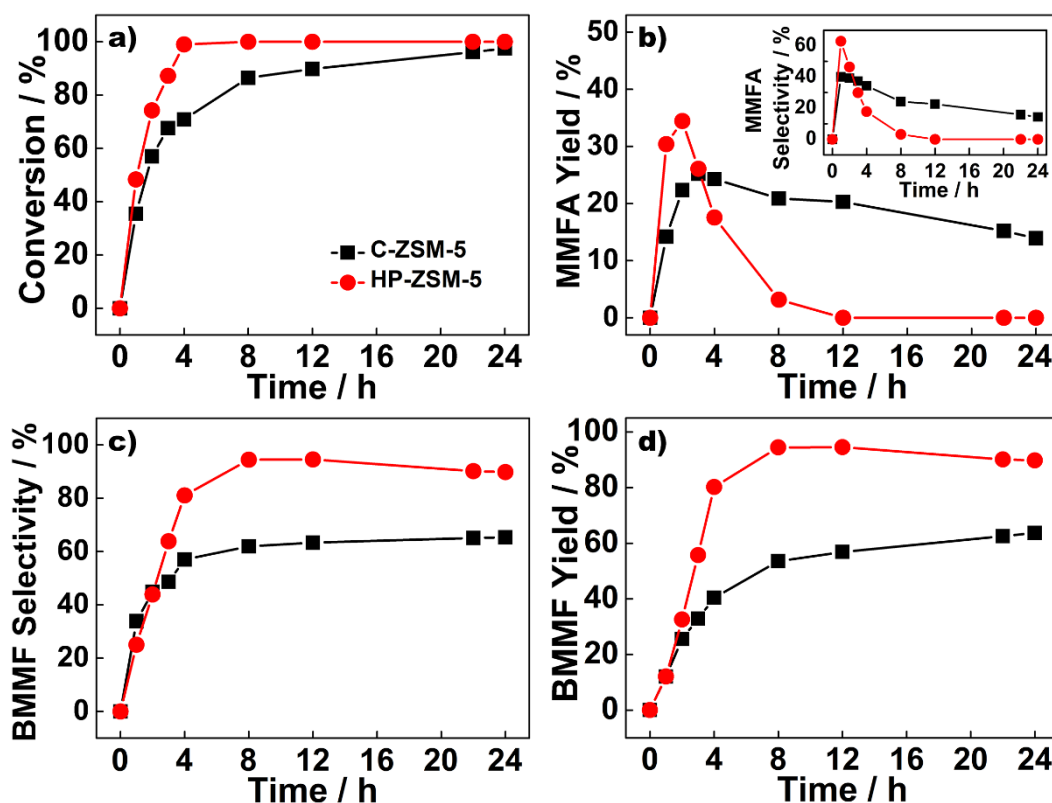


**Figure 1.** Etherification of 2,5-bis(hydroxymethyl)furan (BHMF) with methanol over C-ZSM-5 and HP-ZSM-5. Reaction conditions: 10 g·L<sup>−1</sup> BHMF, 10 g·L<sup>−1</sup> catalyst, 65 °C, 24 h.

## 2.3. Catalyst Reusability

To investigate the deactivation of the catalysts from the coke formation, the spent catalysts were reused under the same condition. As shown in Table 2, the recycled C-ZSM-5 exhibits much lower yield than fresh C-ZSM-5, from 64% to 39.6%, while the recycled HP-ZSM-5 shows slightly lower yield than fresh HP-ZSM-5, from 94.5% to 93.7%. Although only two recycling experiments were conducted, this demonstrates that the coke deposition caused by substrate polymerization within the zeolite pores possibly leads to blocking of the active sites and reduces catalytic activity [26]. Additionally, the deactivation of HP-ZSM-5 is obviously less serious than that of C-ZSM-5, which is tentatively attributed to introduction of mesopores and decreased acidity of HP-ZSM-5.

**Table 2.** Reusability of the C-ZSM-5 and HP-ZSM-5 in the etherification of BHMF <sup>a</sup>.

Catalysts	Time (h)	BMMF Yield (%)
Fresh C-ZSM-5	24	64.0
Spent C-ZSM-5	24	39.6
Fresh HP-ZSM-5	12	94.5
Spent HP-ZSM-5	12	93.7

<sup>a</sup> Reaction conditions: 10 g·L<sup>−1</sup> BHMF, 10 g·L<sup>−1</sup> catalyst, 65 °C.

#### 2.4. Carbon Deposition Analysis

Coke deposition of both spent ZSM-5 was analyzed by Thermogravimetry-Differential Thermal Analysis (TG-DTA) (Figure 2a). The main difference appears above 230 °C, and the weight loss below 230 °C ascribes to the loss of adsorbed water, methanol or some volatile species. Coke deposition over the spent catalysts is completely removed at around 230 °C–700 °C under air atmosphere [27]. It is clear that coke deposition over C-ZSM-5 is higher than that of HP-ZSM-5, indicating that micropores are more likely to be blocked [14]. Combined with the activity of spent catalysts, it is possible to infer that the coke disposition of HP-ZSM-5 is on mesopore walls rather than inside micropores [21], which does not affect catalyst activity.

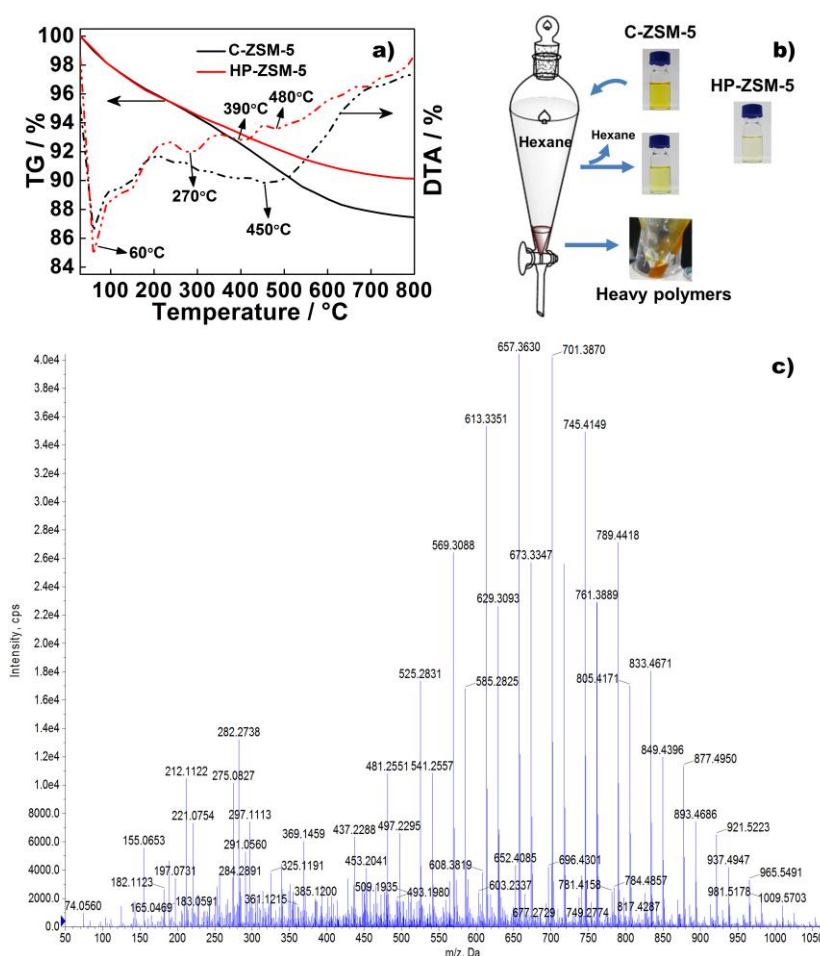


**Figure 2.** (a) Thermogravimetry-Differential Thermal Analysis (TG-DTA) curves of the spent C-ZSM-5 and HP-ZSM-5 under air atmosphere; (b) The separation of heavy polymers; (c) Time-of-Flight Mass Spectrometry (TOF-MS) spectrum of heavy polymers.

The DTA curve of the used C-ZSM-5 shows two main endothermic peaks at around 60 °C and 450 °C. The peak at 60 °C is caused by the volatilization of water, methanol or some volatile species, in line with the TG curve below 230 °C. And the peak at 450 °C is the result of decomposition of polymerization products. On the contrary, there are one main endothermic peak at around 60 °C and three small endothermic peaks at around 270 °C, 390 °C and 480 °C in the DTA curve of HP-ZSM-5. The peak at 60 °C of HP-ZSM-5 is larger than that of C-ZSM-5, suggesting that HP-ZSM-5 contains more absorbed water, methanol or volatile species inside the pore structure. Three small peaks may ascribe to different coke decompositions. All mentioned above indicate that coke deposition is different in two catalysts, which may be attributed to different acidity and pore structure of two catalysts as well as by-products. Besides, coke deposition within C-ZSM-5 may happen not only in the micropores but also on the external surface due to its strong acidity [28].

### 2.5. Speculated Mechanism of Side Reaction during BHMF to BMMF Process

The differences, including catalytic performance, activity of spent catalyst, and coke deposition analysis, between C-ZSM-5 and HP-ZSM-5 demonstrate that acidity and porous structure are two decisive factors in BHMF etherification. Our previous work has already deeply investigated the effect of acidity and improved BMMF yield by adjusting Brønsted and Lewis acidity of catalyst [29]. In this research, the effect of pore structure is investigated by analyzing side reaction mechanism during etherification process, which is beneficial to improve BMMF yield.

Therefore, by-products were separated by purifying crude products. Crude BMMF was obtained after removing methanol, as shown in Figure 2b, it is obvious that color formed by polymerization in HP-ZSM-5 catalytic system is much less than that of C-ZSM-5. Then crude BMMF of C-ZSM-5 was extracted by hexane to obtain purified BMMF. Some deep brown liquid insoluble in hexane was also separated and analyzed by Time-of-Flight Mass Spectrometry (TOF-MS), and then identified as heavy polymers. Molecular weight distribution range of heavy polymers is from 400 Dalton to 1000 Dalton (Figure 2c), which may cause the peak at 450 °C in the DTA curve of C-ZSM-5 as well as coke deposition. The color of purified BMMF (C-ZSM-5) is still darker than that of crude BMMF (HP-ZSM-5), indicating that side reactions also affect the subsequent purification efficiency.

The reaction solutions of C-ZSM-5 and HP-ZSM-5 were further analyzed by Gas Chromatography-Mass Spectrometry (GC-MS) and possible side reaction mechanisms were proposed. As shown in Figure 3, there are different results of reaction solutions catalyzed by C-ZSM-5 and HP-ZSM-5. Since the heavy polymers of C-ZSM-5 catalytic solution couldn't be detected by GC, the GC spectrum of C-ZSM-5 is cleaner than the true fact. The C-ZSM-5 solution still contains more by-products than HP-ZSM-5 solution. Although not all by-products can be identified, some key by-products are confirmed by GC-MS (see Supplementary Materials). 2-(Methoxymethyl)-5-methylene-2,5-dihydrofuran-2-ol (6) and 2,5-dihydro-2-methoxy-2-(methoxymethyl)-5-methylenefuran (7) are identified in solution catalyzed by HP-ZSM-5, and (Z)-6-methoxy-5-oxohex-3-enal (3) is identified in solution catalyzed by C-ZSM-5. Possible side reaction pathways were proposed in terms of the above by-products (Scheme 1).

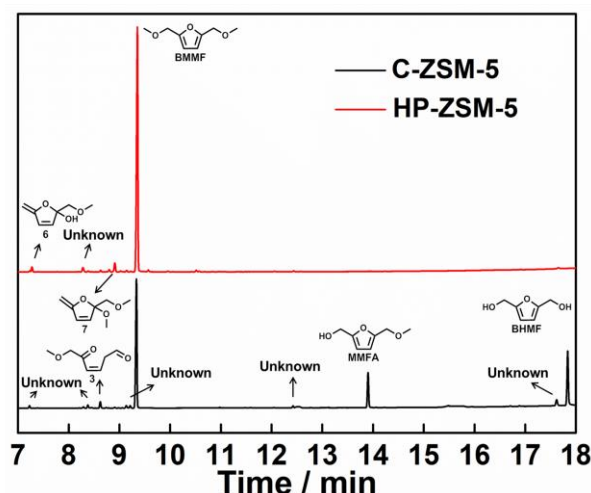
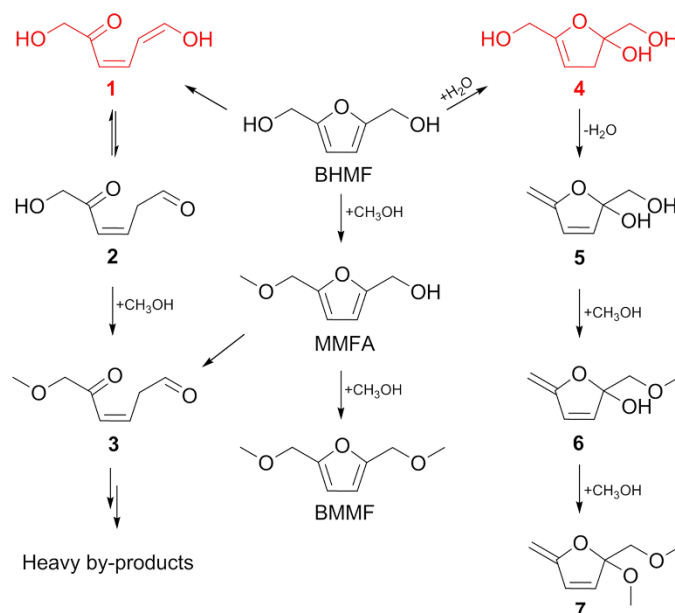


**Figure 3.** Gas Chromatography (GC) spectrum of the by-products on the C-ZSM-5 and HP-ZSM-5. Reaction conditions:  $10 \text{ g} \cdot \text{L}^{-1}$  BHMF,  $10 \text{ g} \cdot \text{L}^{-1}$  catalyst,  $65^\circ \text{C}$ , 12 h.



**Scheme 1.** Proposed mechanism of by-products formation during the BHMF etherification.

The ring-opening reaction of BHMF is easy to occur in the C-ZSM-5 catalytic system due to high acidity of catalyst, and form a conjugated ketone-diene (**1**) which tends to transfer to a steadier aldehyde compound (**2**) [10,16,30–32]. Then **2** gradually etherifies with methanol and converts into **3**, and **3** presumably forms heavy polymers, leading to coke deposition [33]. As for the pathway catalyzed by HP-ZSM-5, hydration reaction is more likely to occur because of catalyst's increased hydrophilia. One C=C double bond of BHMF is prone to hydrate to form **4**, which would influence the other side of the ring [15]. After the loss of water, intermediate **5** generates, and then converts into **6** and **7** through etherifying with methanol.

Since the main differences between C-ZSM-5 and HP-ZSM-5 are porous structure and acidity, distinction of by-products composition is related with these two decisive factors. Introduction of mesopores increases the hydrophilia of catalyst [19], so hydration of BHMF slightly enhances, leading to **4** formation. However, introduction of mesopores also improves mass transport on HP-ZSM-5, which limits transformation of BHMF to ring-opening compounds by shortening transport paths and contact times of substrates inside the channels [24]. Additionally, the relatively weak acidity of



HP-ZSM-5 suppresses the ring-opening reaction and subsequent side reactions. Thus, both decreased acidity and mesoporous structure contribute to the high selectivity and yield of BMMF over HP-ZSM-5.

### 3. Material and Methods

#### 3.1. Materials

Tetraethyl orthosilicate (TEOS), aluminum isopropoxide (AIP), tetrapropylammonium hydroxide (TPAOH), ethanol (EtOH), and methanol (MeOH) were purchased from Sinopharm Chemical Reagent Co., Ltd. (Shanghai, China) Trifluoroacetic acid ( $\text{CF}_3\text{COOH}$ ) and hexadecyltrimethoxysilane (HTS) were obtained from Aladdin Industrial Inc. (Shanghai, China) BHMF, MMFA and BMMF were purchased from Ningbo Biomass and Biotechnology Co., Ltd. (Ningbo, China, [www.nbbiotech.com](http://www.nbbiotech.com)) C-ZSM-5 was obtained from Nankai University Catalyst Co. Ltd. (Tianjin, China) All chemicals were used without further purification in this work.

#### 3.2. Synthesis of Catalysts

HP-ZSM-5 was synthesized by a solvent-evaporation-assisted dry-gel conversion method [19]. For the synthesis, TEOS, AIP, TPAOH, HTS, and ethanol were mixed in a molar ratio of  $1\text{SiO}_2$ :  $0.01\text{Al}_2\text{O}_3$ :  $0.2\text{TPAOH}$ :  $0.05\text{HTS}$ :  $15\text{EtOH}$ . Ethanol was first poured into a 100 mL beaker. AIP, TPAOH, HTS, and TEOS were slowly added when the solvent was stirring (600 rpm, r.t.). In order to evaporate ethanol, the resulting gel was aged at room temperature for three days, and then placed in a poly(tetrafluoroethylene) (PTFE) cup before transferring into a Teflon-lined autoclave. A small amount of water was added outside the cup to create steam, and the autoclave was heated at  $175\text{ }^\circ\text{C}$  for 72 h. After crystallization, the product was filtered and washed with deionized water, then calcined at  $550\text{ }^\circ\text{C}$  for 6 h to obtain the HP-ZSM-5.

#### 3.3. Catalysts Characterization

XRD patterns were recorded on a Bruker D8 ADVANCE X-ray diffractometer (Bruker Corporation, Karlsruhe, Germany) using  $\text{Cu K}\alpha$  radiation at 40 kV and 40 mV with scanning angle ( $2\theta$ ) from  $5^\circ$  to  $80^\circ$ . Nitrogen adsorption and desorption isotherms were performed at  $-196\text{ }^\circ\text{C}$  by using a Micromeritics ASAP-2020 system (Micromeritics Instrument Corp., Norcross, GA, USA). Before physisorption measurements, all samples were outgassed under vacuum at  $300\text{ }^\circ\text{C}$  for 10 h. The total surface areas and micropore volumes were evaluated by the BET method and the t-plot method, respectively. The total pore volumes were estimated from the amount of  $\text{N}_2$  adsorbed at  $P/P_0 = 0.99$  and the meso-/macro-pore volumes were determined by subtracting micropore volumes from total pore volumes. The Barret–Joyner–Halenda (BJH) model was employed to calculate the poresize distribution of the samples. The chemical compositions of Al and Si were determined by X-ray fluorescence spectroscopy on a ZSX Primus II instrument (Rigaku Corporation, Tokyo, Japan). Temperature-programmed desorption of ammonia ( $\text{NH}_3$ -TPD) of the samples was performed by using a Micromeritics Auto Chem II 2920 chemisorption instrument (Micromeritics Instrument Corp., Norcross, GA, USA) equipped with a thermal conductivity detector (TCD). Typically, 0.1 g of the samples was first degassed at  $600\text{ }^\circ\text{C}$  for 1 h at a  $30\text{ mL}\cdot\text{min}^{-1}$  flow rate of Helium purge gas and then cooled down to  $100\text{ }^\circ\text{C}$ . The adsorption of  $\text{NH}_3$  was performed with a 10%  $\text{NH}_3$ /90% Helium mixture at a rate of  $50\text{ mL}\cdot\text{min}^{-1}$  for 1 h to obtain the samples saturation with ammonia. After  $\text{NH}_3$  adsorption, the gas mixture was switched back to Helium, and the zeolite was purged at  $100\text{ }^\circ\text{C}$  for 1 h to remove the weakly adsorbed  $\text{NH}_3$ . The desorption of  $\text{NH}_3$  was conducted between  $100\text{ }^\circ\text{C}$  and  $600\text{ }^\circ\text{C}$  with a heating rate of  $10\text{ }^\circ\text{C}\cdot\text{min}^{-1}$  under Helium flow.

#### 3.4. Catalytic Activity

The etherification of BHMF was evaluated in a 250 mL two-neck flask under atmospheric pressure at  $65\text{ }^\circ\text{C}$  on an IKA RCT Basic stir (IKA-Werke GmbH&Co. KG, Staufen, Germany) plate equipped

with a thermocouple to monitor the solution temperature. In a typical run, mixture of BHMF (0.8 g, 6.25 mmol), catalyst (0.8 g) and methanol (80 mL) were added (600 rpm). After a certain period of reaction time, the reaction mixture was cooled to room temperature. Then the catalyst was separated by centrifugation. The product was analyzed after diluting with deionized water.

### 3.5. Product Analysis

The quantitative analyzes of BHMF, MMFA and BMMF were analyzed by an Agilent 1260 HPLC Infinity instrument (Agilent Technologies Co., Ltd., Waldbronn, Germany) equipped with an UV detector at 220 nm and an Agilent ZORBAX SB-C<sub>18</sub> column (Agilent Technologies Co., Ltd., Waldbronn, Germany) at 30 °C. A mixture of methanol (25%, v/v) and a 0.5% CF<sub>3</sub>COOH (75%, v/v) solution flowing at 1 mL·min<sup>−1</sup> was employed as the mobile phase. The contents of BHMF, MMFA and BMMF were calculated using an external standard method. The definitions of BHMF conversion and product yields are as follows: BHMF conversion (mol %) = (1-moles of BHMF in product/moles of initial BHMF) \* 100%; Product yield (mol %) = (moles of product produced/moles of initial BHMF) \* 100%; Product selectivity (mol %) = product yield/BHMF conversion \* 100%; Mass balance = (moles of initial BHMF-moles of BHMF in product-moles of MMFA produced-moles of BMMF produced)/moles of initial BHMF \* 100%. The coke deposition of catalysts was conducted on a PerkinElmer Diamond TG/DTA at a heating rate of 10 °C·min<sup>−1</sup> from 30 °C to 800 °C in air flow. The by-products were confirmed by a combination of GC-MS and TOF-MS. GC-MS analysis was performed on an Agilent GC-MS 7890B-5977A (Agilent Technologies Co., Ltd., Waldbronn, Germany) equipped with Agilent DB-WAX UI column (Agilent Technologies Co., Ltd., Waldbronn, Germany) with a quadrupole mass analyzer using helium as the carrier gas. TOF-MS analysis was conducted on an AB Sciex TripleTOF®4600 (AB Sciex Pte. Ltd., Redwood City, CA, USA). Extraction was performed by using a separation funnel (volumes of crude product/volumes of hexane, 1/30). The objective phase is crude product (C-ZSM-5) and the extracted phase is hexane. After extraction equilibrium was attained, the two phases were separated, and the supernatant was by-products.

## 4. Conclusions

In this paper, different by-products of C-ZSM-5 and HP-ZSM-5 were identified, which affects catalytic performance. Based on the previous reports and our results, two possible mechanisms of side reaction pathways were tentatively proposed during etherification. HP-ZSM-5 exhibited excellent catalytic activity and high selectivity, because relatively weak acidity of HP-ZSM-5 could suppress the ring-opening reaction and subsequent side reactions. Introduction of mesopores in HP-ZSM-5 not only improves mass transport but also slightly increases hydration of BHMF. This work provides some key clues to further improve BMMF yield, especially by suppressing hydrate reaction of HP-ZSM-5.

**Supplementary Materials:** The following are available online at <http://www.mdpi.com/2073-4344/8/9/383/s1>. Figure S1: X-ray diffraction patterns of the catalysts. (HP-ZSM-5: hierarchical porous ZSM-5; C-ZSM-5: conventional ZSM-5.), Figure S2: N<sub>2</sub> physisorption isotherms of the samples and the Barrett-Joyner-Halenda adsorption pore size distributions of the catalysts (inside), Figure S3: Temperature-programmed desorption of ammonia profiles of the samples, Figure S4: Mass spectrum corresponding to the peak of compound 6 in Figure 3, Figure S5: Mass spectrum corresponding to the peak of compound 7 in Figure 3, Figure S6: Mass spectrum corresponding to the peak of compound 3 in Figure 3.

**Author Contributions:** Y.Z. and L.W. conceived and designed the experiments; W.F. performed the experiments; W.F. and H.H. analyzed the data; W.F. and Z.M. contributed reagents/materials/analysis tools; W.F. and Y.Z. wrote the paper.

**Acknowledgments:** This work was supported by National Key Technology Research and Development Program of the Ministry of Science and Technology of China (No. 2015BAD15B08) and Ningbo Science and Technology Bureau (No. 2015B11004).

**Conflicts of Interest:** The authors declare no conflicts of interest.



## References

1. De Jong, E.; Vijlbrief, T.; Hijkoop, R.; Gruter, G.J.M.; van der Waal, J.C. Promising results with YXY Diesel components in an ESC test cycle using a PACCAR Diesel engine. *Biomass Bioenergy* **2012**, *36*, 151–159. [\[CrossRef\]](#)
2. Mascal, M.; Nikitin, E.B. Direct, high-yield conversion of cellulose into biofuel. *Angew. Chem. Int. Ed.* **2008**, *47*, 7924–7926. [\[CrossRef\]](#) [\[PubMed\]](#)
3. Tang, X.; Wei, J.; Ding, N.; Sun, Y.; Zeng, X.; Hu, L.; Liu, S.; Lei, T.; Lin, L. Chemoselective hydrogenation of biomass derived 5-hydroxymethylfurfural to diols: Key intermediates for sustainable chemicals, materials and fuels. *Renew. Sustain. Energy Rev.* **2017**, *77*, 287–296. [\[CrossRef\]](#)
4. Gruter, G.M.J. Hydroxymethylfurfural Ethers From Sugars or HMF and Branched Alcohols. U.S. 20100218416A1, 2 September 2010.
5. Lee, Y.; Kim, J.; Han, J.; Kim, Y.; Jung, B.; Hwang, S.; Jegal, J. Highly selective catalytic hydrogenation and etherification of 5-hydroxymethyl-2-furaldehyde to 2,5-bis(alkoxymethyl)furans for potential biodiesel production. *Synlett* **2017**, *28*, 2299–2302.
6. Cao, Q.; Liang, W.Y.; Guan, J.; Wang, L.; Qu, Q.; Zhang, X.Z.; Wang, X.C.; Mu, X.D. Catalytic synthesis of 2,5-bis-methoxymethylfuran: A promising cetane number improver for diesel. *Appl. Catal. A Gen.* **2014**, *481*, 49–53. [\[CrossRef\]](#)
7. Gupta, D.; Saha, B. Dual acidic titania carbocatalyst for cascade reaction of sugar to etherified fuel additives. *Catal. Commun.* **2018**, *110*, 46–50. [\[CrossRef\]](#)
8. Li, X.L.; Zhang, K.; Chen, S.Y.; Li, C.; Li, F.; Xu, H.J.; Fu, Y. A cobalt catalyst for reductive etherification of 5-hydroxymethyl-furfural to 2,5-bis (methoxymethyl)furan under mild conditions. *Green Chem.* **2018**, *20*, 1095–1105. [\[CrossRef\]](#)
9. Li, H.; Yang, S.; Riisager, A.; Pandey, A.; Sangwan, R.S.; Saravanamurugan, S.; Luque, R. Zeolite and zeotype-catalysed transformations of biofuranic compounds. *Green Chem.* **2016**, *18*, 5701–5735. [\[CrossRef\]](#)
10. Wang, H.; Frenklach, M. Transport properties of polycyclic aromatic hydrocarbons for flame modeling. *Combust. Flame* **1994**, *96*, 163–170. [\[CrossRef\]](#)
11. Jae, J.; Tompsett, G.A.; Foster, A.J.; Hammond, K.D.; Auerbach, S.M.; Lobo, R.F.; Huber, G.W. Investigation into the shape selectivity of zeolite catalysts for biomass conversion. *J. Catal.* **2011**, *279*, 257–268. [\[CrossRef\]](#)
12. Park, H.J.; Park, K.H.; Jeon, J.K.; Kim, J.; Ryoo, R.; Jeong, K.E.; Park, S.H.; Park, Y.K. Production of phenolics and aromatics by pyrolysis of miscanthus. *Fuel* **2012**, *97*, 379–384. [\[CrossRef\]](#)
13. Lee, H.I.; Park, H.J.; Park, Y.K.; Hur, J.Y.; Jeon, J.K.; Kim, J.M. Synthesis of highly stable mesoporous aluminosilicates from commercially available zeolites and their application to the pyrolysis of woody biomass. *Catal. Today* **2008**, *132*, 68–74. [\[CrossRef\]](#)
14. Xian, X.; Ran, C.; Nai, C.; Yang, P.; Zhao, S.; Dong, L. Characterization of the location of coke deposited on spent HZSM-5 zeolite by special temperature-programmed oxidation and isothermal oxidation methods. *Appl. Catal. A Gen.* **2017**, *547*, 37–51. [\[CrossRef\]](#)
15. Gelmini, A.; Albonetti, S.; Cavani, F.; Cesari, C.; Lolli, A.; Zanotti, V.; Mazzoni, R. Oxidant free one-pot transformation of bio-based 2,5-bis-hydroxymethylfuran into  $\alpha$ -6-hydroxy-6-methyl-4-enyl-2H-pyran-3-one in water. *Appl. Catal. B Environ.* **2016**, *180*, 38–43. [\[CrossRef\]](#)
16. Alamillo, R.; Tucker, M.; Chia, M.; Pagán Torres, Y.; Dumesic, J. The selective hydrogenation of biomass-derived 5-hydroxymethylfurfural using heterogeneous catalysts. *Green Chem.* **2012**, *14*, 1413–1419. [\[CrossRef\]](#)
17. Rosatella, A.A.; Simeonov, S.P.; Frade, R.F.M.; Afonso, C.A.M. 5-Hydroxymethylfurfural (HMF) as a building block platform: Biological properties, synthesis and synthetic applications. *Green Chem.* **2011**, *13*, 754–793. [\[CrossRef\]](#)
18. Chuntanapum, A.; Matsumura, Y. Formation of Tarry Material from 5-HMF in Subcritical and Supercritical Water. *Ind. Eng. Chem. Res.* **2009**, *48*, 9837–9846. [\[CrossRef\]](#)
19. Zhu, K.; Sun, J.M.; Liu, J.; Wang, L.Q.; Wan, H.Y.; Hu, J.Z.; Wang, Y.; Peden, C.H.F.; Nie, Z.M. Solvent evaporation assisted preparation of oriented nanocrystalline mesoporous MFI zeolites. *ACS Catal.* **2011**, *1*, 682–690. [\[CrossRef\]](#)
20. Sing, K.S.W. Reporting physisorption data for gassolid systems with special reference to the determination of surface area and porosity. *Pure Appl. Chem.* **1982**, *154*, 2201–2218. [\[CrossRef\]](#)

21. Kim, J.N.; Choi, M.; Ryoo, R. Effect of mesoporosity against the deactivation of MFI zeolite catalyst during the methanol-to-hydrocarbon conversion process. *J. Catal.* **2010**, *269*, 219–228. [[CrossRef](#)]
22. Serrano, D.P.; García, R.A.; Vicente, G.; Linares, M.; Procházková, D.; Čejka, J. Acidic and catalytic properties of hierarchical zeolites and hybrid ordered mesoporous materials assembled from MFI protozeolitic units. *J. Catal.* **2011**, *279*, 366–380. [[CrossRef](#)]
23. Serrano, D.P.; Escola, J.M.; Pizarro, P. Synthesis strategies in the search for hierarchical zeolites. *Chem. Soc. Rev.* **2013**, *42*, 4004–4035. [[CrossRef](#)] [[PubMed](#)]
24. Sazama, P.; Sobalik, Z.; Dedeczek, J.; Jakubec, I.; Parvulescu, V.; Bastl, Z.; Rathousky, J.; Jirglova, H. Enhancement of activity and selectivity in acid-catalyzed reactions by dealuminated hierarchical zeolites. *Angew. Chem. Int. Ed.* **2013**, *52*, 2038–2041. [[CrossRef](#)] [[PubMed](#)]
25. Holm, M.S.; Taarning, E.; Egeblad, K.; Christensen, C. Catalysis with hierarchical zeolites. *Catal. Today* **2011**, *168*, 3–16. [[CrossRef](#)]
26. Koehle, M.; Lobo, R.F. Lewis acidic zeolite Beta catalyst for the Meerwein-Ponndorf-Verley reduction of furfural. *Catal. Sci. Technol.* **2016**, *6*, 3018–3026. [[CrossRef](#)]
27. Gou, M.L.; Cai, J.Q.; Song, W.S.; Liu, Z.; Ren, Y.L.; Pan, B.L.; Niu, Q.S. Coking and deactivation behavior of ZSM-5 during the isomerization of styrene oxide to phenylacetaldehyde. *Catal. Commun.* **2017**, *98*, 116–120. [[CrossRef](#)]
28. Gou, J.S.; Wang, Z.P.; Li, C.; Qi, X.D.; Vattipalli, V.; Cheng, Y.T.; Huber, G.; Conner, W.C.; Dauenhauer, P.J.; Mountziaris, T.J.; Fan, W. The effects of ZSM-5 mesoporosity and morphology on the catalytic fast pyrolysis of furan. *Green Chem.* **2017**, *19*, 3549–3557. [[CrossRef](#)]
29. Fang, W.T.; Hu, H.L.; Dong, P.; Ma, Z.S.; He, Y.L.; Wang, L.; Zhang, Y.J. Improvement of furanic diether selectivity by adjusting Brønsted and Lewis acidity. *Appl. Catal. A Gen.* **2018**, *565*, 146–151. [[CrossRef](#)]
30. Shindo, A.; Izumino, K. Structural variation during pyrolysis of furfuryl alcohol and furfural-furfuryl alcohol resins. *Carbon* **1994**, *32*, 1233–1243. [[CrossRef](#)]
31. Horvat, J.; Klaić, B.; Metelko, B.; Šunjić, V. Mechanism of levulinic acid formation. *Tetrahedron Lett.* **1985**, *26*, 2111–2114. [[CrossRef](#)]
32. Wahlen, J.; Moens, B.; De Vos, D.E.; Alsters, P.L.; Jacobs, P.A. Titanium silicalite 1 (TS-1) catalyzed oxidative transformations of furan derivatives with hydrogen peroxide. *Adv. Synth. Catal.* **2004**, *346*, 333–338. [[CrossRef](#)]
33. Che, P.; Lu, F.; Zhang, J.; Huang, Y.; Nie, X.; Gao, J.; Xu, J. Catalytic selective etherification of hydroxyl groups in 5-hydroxymethylfurfural over H<sub>4</sub>SiW<sub>12</sub>O<sub>40</sub>/MCM-41 nanospheres for liquid fuel production. *Bioresour. Technol.* **2012**, *119*, 433–436. [[CrossRef](#)] [[PubMed](#)]



© 2018 by the authors. Licensee MDPI, Basel, Switzerland. This article is an open access article distributed under the terms and conditions of the Creative Commons Attribution (CC BY) license (<http://creativecommons.org/licenses/by/4.0/>).